Correlating Stiffness, Ductility, and Morphology of Polymer:Fullerene Films for Solar Cell Applications

ARTICLE *in* ADVANCED ENERGY MATERIALS · MARCH 2013

Impact Factor: 16.15 · DOI: 10.1002/aenm.201200595

6 AUTHORS, INCLUDING:

Omar Awartani
Organic and Carbon Electronics Laboratory…
5 PUBLICATIONS **28** CITATIONS
SEE PROFILE

Hyun Wook Ro
National Institute of Standards and Techno…
63 PUBLICATIONS **971** CITATIONS
SEE PROFILE

Lee Richter
National Institute of Standards and Techno…
166 PUBLICATIONS **6,029** CITATIONS
SEE PROFILE

Brendan O'Connor
North Carolina State University
25 PUBLICATIONS **510** CITATIONS
SEE PROFILE

ADVANCED ENERGY MATERIALS
www.advenergymat.de

Correlating Stiffness, Ductility, and Morphology of Polymer:Fullerene Films for Solar Cell Applications

Omar Awartani, Bethany I. Lemanski, Hyun Wook Ro, Lee J. Richter, Dean M. DeLongchamp, and Brendan T. O'Connor**

The development of flexible and physically robust organic solar cells requires detailed knowledge of the mechanical behavior of the heterogeneous material stack. However, in these devices there has been limited research on the mechanical properties of the active organic layer. Here, two critical mechanical properties, stiffness and ductility, of a widely studied organic solar cell active layer, a blend film composed of poly(3-hexylthiophene) (P3HT) and [6,6]-phenyl C61-butyric acid methyl ester (PCBM) are reported. Processing conditions are varied to produce films with differing morphology and correlations are developed between the film morphology, mechanical properties and photovoltaic device performance. The morphology is characterized by fitting the absorption of the P3HT:PCBM films to a weakly interacting H-aggregate model. The elastic modulus is determined using a buckling metrology approach and the crack onset strain is determined by observing the film under tensile strain using optical microscopy. Both the elastic modulus and crack onset strain are found to vary significantly with processing conditions. Processing methods that result in improved device performance are shown to decrease both the compliance and ductility of the film.

1. Introduction

Advancements in power conversion efficiency continue to be made in organic solar cells pushing this technology closer to widespread commercial implementation.[1,2] It is likely that many initial applications will require exploitation of the unique attribute of flexibility afforded by this technology. While organic photovoltaic (OPV) research is focused on materials synthesis,[3] photophysics,[4] and morphology-optoelectronic performance relationships,[5,6] mechanical robustness is also critical for commercial success. As a device is flexed during fabrication and operation, the heterogeneous material stack must withstand the resulting strains and continue to perform effectively. Research in this area has been focused on similarly structured organic light emitting device (OLED) technology.[7] Significant work has been done on the mechanical behavior of plastic substrates,[8] encapsulation,[9] and electrodes.[10,11] However, there has been little research on the mechanical behavior of the active organic semiconductor layers.[12–14] In this report, we determine the elastic modulus and crack onset strain of a widely studied organic solar cell active layer, the bulk heterojunction (BHJ) thin film composed of poly(3-hexylthiophene) (P3HT) and [6,6]-phenyl C61-butyric acid methyl ester (PCBM).[15,16] Stiffness and ductility are key properties that can provide insight into mechanical failure mechanisms of the active layer.[17] Previous research on the mechanical behavior of P3HT:PCBM blend films include analysis of adhesion,[12] hardness,[14] and stiffness.[13,18] While the elastic modulus was previously reported, a detailed analysis that considered morphological differences was not provided.[13] Of particular interest here is determining how the BHJ morphology, which is known to impact optoelectronic behavior,[19,20] is reflected in the stiffness and ductility of the film. Understanding how the morphology of the active layer relates to both the electrical and mechanical behavior will assist in the development of flexible and physically robust organic solar cells.

In P3HT:PCBM organic photovoltaic (OPV) devices, the polymer and fullerene derivative are typically dissolved in a common solvent at a 1:1 ratio by mass. The solution is then spun cast to form a thin film (~200 nm) in which the two materials spatially segregate on a nm length scale. It is well known that processing methods can strongly influence the morphology of P3HT:PCBM films, which in turn dictates OPV device performance.[1,16,19] While, the morphological picture of P3HT:PCBM solar cells has been widely studied, intricacies of the morphology are continuing to evolve.[5,21] The widely accepted morphological picture is that the blend film consists of regions of crystalline P3HT with negligible PCBM intercalation, and a mixed amorphous P3HT:PCBM phase.[5] The materials may also vertically segregate within the film depending on interfacial surface energy and film thickness.[22,23] There has

O. Awartani, Prof. B. T. O'Connor
Department of Mechanical and Aerospace Engineering
North Carolina State University, Raleigh, NC 27695, USA
E-mail: brendan_oconnor@ncsu.edu
B. I. Lemanski
Department of Mechanical Engineering
Massachusetts Institute of Technology
Cambridge, MA 02139, USA
Dr. H. W. Ro, Dr. L. J. Richter, Dr. D. M. DeLongchamp
Materials Measurement Laboratory
National Institute of Standards and Technology
Gaithersburg, MD 20899, USA
E-mail: dean.delongchamp@nist.gov

DOI: 10.1002/aenm.201200595

been a wide range of processing methods used to optimize the morphology of the blend film including thermal annealing,[19,24] solvent annealing,[16,24] and/or the use of solvent additives.[25,26] These processing conditions have been shown to increase P3HT crystallinity and improve the P3HT local order.

The focus of this work is to determine how the variation in the film morphology influences not only the OPV device performance but also the mechanical properties of the blend film. To vary the film morphology while keeping the film at device relevant thicknesses (~215 ± 10 nm), a range of P3HT:PCBM solution concentrations and spin coating speeds are used. Spin speed is primarily used to vary the level of order within the film while solution concentration is used to ensure proper film thickness. In addition to casting method, post-cast treatment by solvent and thermal annealing is used to further tune the film morphology. All BHJ films are cast on poly(3,4-ethylenedioxythiophene):poly(styrenesulfonate) (PEDOT:PSS) coated silicon or ITO-glass substrates, depending on the subsequent measurements on the film. We focus on six unique P3HT:PCBM blend films with their processing parameters summarized in **Table 1**. We also consider neat P3HT and PCBM films for comparison with the blend films.

The mechanical properties of the BHJ films were measured by physically manipulating the films on a poly(dimethylsiloxane) PDMS substrate. The elastic modulus was determined using a buckling metrology approach.[27] This method consists of placing a compressive strain on the thin film-PDMS stack resulting in a characteristic buckling pattern. An example of the buckling pattern for a P3HT:PCBM blend film is given in **Figure 1**, and an illustration of the buckling process is given in Figure 4. Once the film is buckled, the elastic modulus (E) is determined by $\bar{E}_f = 3\bar{E}_s(\lambda_B/2\pi h_f)^3$ where, λ_B is the buckling wavelength, h_f is the film thickness, and the plane-strain modulus is $\bar{E} = E(1-\nu^2)$ where ν is Poisson's ratio.[27] The subscripts f and s refer to the thin film and substrate, respectively.

Table 1. List of processing conditions for the films under study. All materials were dissolved in dichlorobenzene and cast at room temperature. The annealing process consisted of placing the films in an enclosed Petri dish for 20 minutes followed by thermally annealing at 110 C for 20 minutes. Additional details of the processing conditions are provided in the experimental section.

P3HT:PCBM film type	Solution (mg/ml)	Spin speed (rpm)	Thickness (nm)	Post cast Treatment
1	45	2,000	204–216	As cast
2	45	2,000	204–220	Annealed
3	36	1,000	210–223	As cast
4	36	1,000	218–225	Annealed
5	30	600	214–228	As cast
6	30	600	215–234	Annealed
Neat P3HT film	20	1,000	155–158	Both
Neat PCBM film	30	1,000	73–76	Both

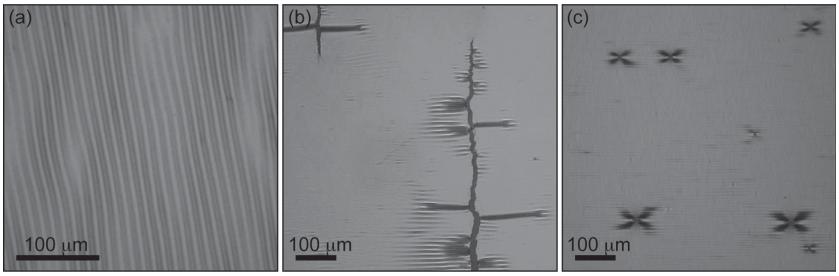

Figure 1. Optical micrographs of P3HT:PCBM blend films. (a) Typical buckling pattern for P3HT:PCBM film on PDMS under compression (film type 6). P3HT:PCBM films showing fracture characteristic for (b) film type 6 and (c) film type 3. The difference in crack features is indicative of the difference in ductility between films.

The elastic modulus of the PDMS is measured using a tensile tester and varied between 0.66 MPa and 0.73 MPa. Poisson's ratio of PCBM is expected to be similar to C_{60}, which has been reported as 0.36.[28] Poisson's ratio of P3HT has been estimated to be approximately 0.35.[18] Therefore, Poisson's ratio of all thin films is taken as 0.35 and Poisson's ratio of PDMS is taken as 0.5.[27,29] The average elastic modulus is determined by measuring a minimum of 3 films for each processing condition. To determine the crack onset strain, the film is strained on PDMS in tension until cracks are observed under an optical microscope.[29,30] The average crack onset strain is determined by measuring a minimum of 4 films for the blend films, and a minimum of 2 films for the neat films. Images showing characteristic fracture behavior in the P3HT:PCBM films are provided in Figure 1.

2. Results and Discussion

2.1. Film Morphology and OPV Device Performance

There have been a number of approaches used to characterize the morphology of P3HT:PCBM films in detail including X-ray scattering and electron microscopy, among others.[5,31,32] While many features of the morphology have been uncovered, a complete picture remains under development. Elucidating the precise morphology is beyond the scope of this work and to determine differences in film morphology we turn to a simple, yet effective, approach of measuring the absorbance of the film with a UV-visible spectrometer.[20] The normalized absorbance spectrum of the various BHJ films under study is provided in **Figure 2**. The absorbance spectrum over the visible range is dominated by P3HT with characteristic vibronic peaks at 550 nm and 605 nm.[33,34] Qualitatively, a decrease in the ratio of the 550 nm absorbance peak to the 605 nm peak correlates to an increase in the P3HT local order.[33,35] Quantitatively, the absorption spectrum represents a complex interplay between the interchain and intrachain coupling.[33] Recently, the absorption of P3HT has been successfully modeled based on H-aggregates comprised of co-facially packed conjugated chains in the case of weak excitonic coupling.[20,33,35] This model is applied here to provide quantitative estimates of the fraction of aggregate P3HT in the blend, as well as the average conjugation

DOI: 10.1002/aenm.201200595

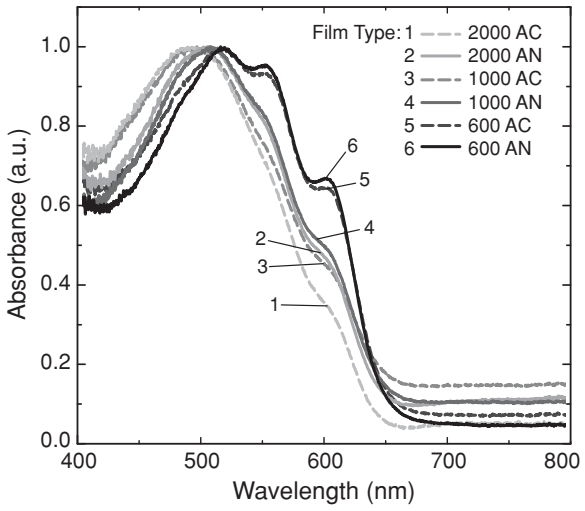

Figure 2. Normalized absorbance measurements of P3HT:PCBM films for various processing conditions. Legend, the film type is given in Table 1, the following number refers to spin cast speed, AC is for as-cast and AN is for annealed films.

Film Type	j_{SC} (mA/cm^2)	Voc (V)	FF	η (%)
1	3.22	0.65	0.69	1.44
2	5.63	0.60	0.67	2.23
3	4.10	0.64	0.67	1.76
4	6.76	0.59	0.67	2.67
5	7.89	0.60	0.67	3.13
6	9.91	0.57	0.66	3.67

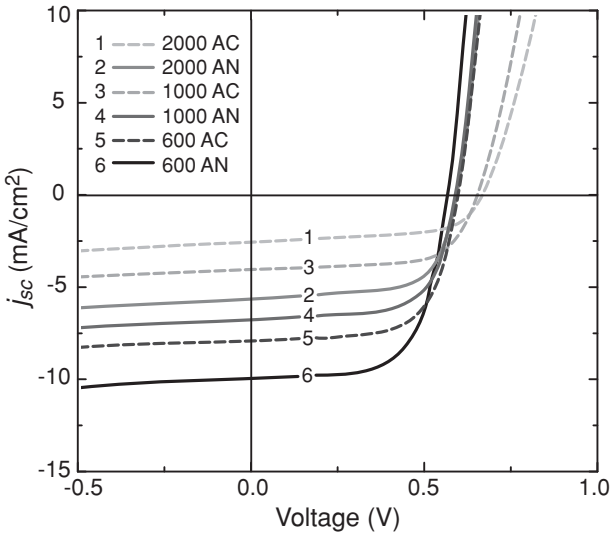

Figure 3. Top, the performance results for the 6 films under study, with processing methods given in Table 1. Reported results include the short circuit current (j_{sc}), open circuit voltage (V_{OC}), fill factor (FF), and power conversion efficiency (η). Bottom, current-voltage curves for the 6 films under 1-sun illumination conditions.

length and quality of the aggregates. The absorption model fitting parameters include the exciton bandwidth (W), the Gaussian line width (σ), and the $0 \rightarrow 0$ transition energy (E_{00}). W is a measure of the length of interacting chain segments forming the P3HT aggregate, and σ is a measure of the local interchain order. The fraction of aggregate P3HT in the blend is determined by modeling the contribution of aggregate P3HT to the total absorption spectrum.[20,35] Further information on the absorption model and fit to the experimental absorbance data is provided in the Supplemental Information. The best-fit values of W, σ, E_{00}, and the estimated percentage of aggregate P3HT in the blend films under study are given in Table S1. The percentage of aggregate P3HT in the blend films is estimated to range from 35% to 51%. This estimate is based on the absorbance over the wavelength range of 400 nm to 750 nm and thus does not account for absorption of amorphous P3HT below 400 nm. The unaccounted absorption results in a slight overestimate of the percent aggregate P3HT in the films; however, the trend in the change of aggregate P3HT between films is expected to remain.

While the absorption parameters are associated with aggregate P3HT, they also provide indirect information about the blend film. It has been shown that P3HT crystals are largely free of intercalated PCBM.[36] Thus, as processing methods are used to improve P3HT crystallinity, a higher concentration of PCBM is distributed throughout the amorphous P3HT region. The increase in P3HT crystallinity has also been shown to result in an increase in the electron mobility in the BHJ film, suggesting improved molecular connectivity of the PCBM in the mixed P3HT:PCBM phase.[20] Finally, it has been shown that for similarly processed films, there is no substantial crystallization of the PCBM.[5,21,37]

Organic solar cells were fabricated using the different P3HT:PCBM processing conditions summarized in Table 1, resulting in a large variation in device performance. In this study we focused on the BHJ film thickness that gives the highest power conversion efficiency of 3.7%, which is a film approximately 220 nm thick. As seen in **Figure 3**, the difference in power conversion efficiency is largely driven by the change in short circuit current. To determine if the slight thickness variation, given in Table 1, causes a large change in the optical field intensity distribution in the active layer and thus contributes significantly to the observed differences in performance, the solar cells were modeled using a transfer matrix optical model.[39] The change in short circuit current is determined by assuming an internal quantum efficiency of 70% for the BHJ over the incident light wavelength range of 300 to 800 nm. Using previously reported optical constants for each layer,[38,39] the change in short circuit current due to thickness is predicted to be less than 7% and does not account for the large change in device performance observed. Therefore the change in performance is attributed to changes in the morphology of the P3HT:PCBM film. This difference in device performance is expected, where similar changes in absorbance characteristics have been correlated with the OPV external quantum efficiency.[40]

2.2. Elastic Modulus

The elastic modulus of the various P3HT:PCBM films was measured along with the elastic modulus of neat P3HT and

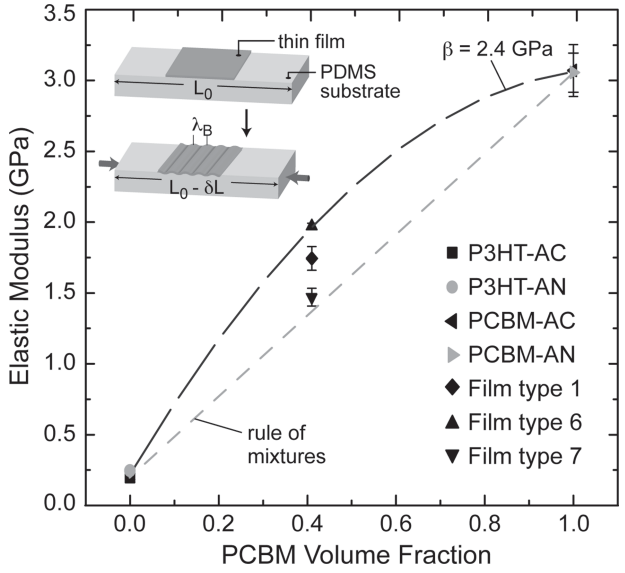

Figure 4. Elastic modulus of BHJ films with variation in PCBM volume fraction. The volume fraction was determined based on a density of P3HT of 1.1 g cm^{-3} and PCBM of 1.6 g cm^{-3}.[21] The values are plotted along with the line for the rule of mixtures, and for the synergistic modulus with interaction term $\beta = 2.4$ GPa. The P3HT:PCBM film type 7 is a film cast from 38 mg ml^{-1} solution, spun cast at 2,000 rpm without post cast annealing. Inset, an illustration of the buckling process used to determine the elastic modulus of the thin films.

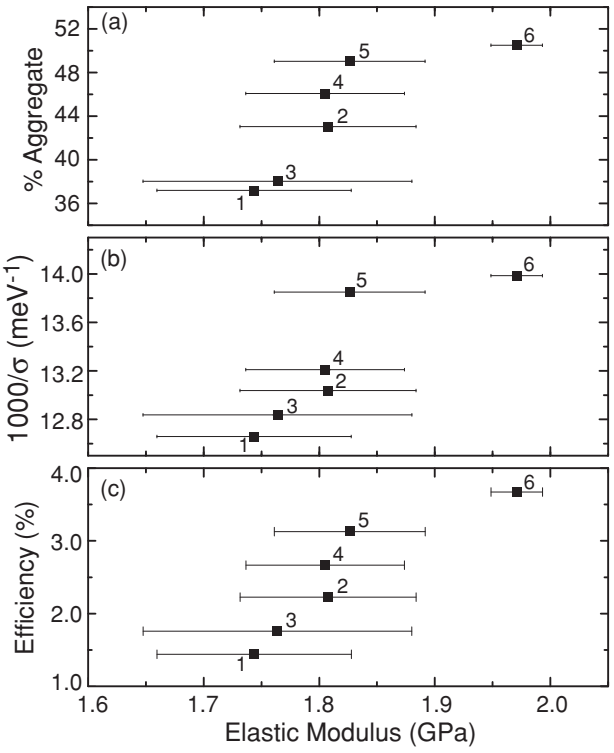

Figure 5. (a-b) Correlations between the elastic modulus and morphology characteristics of P3HT:PCBM blend films including (a) the percent aggregate P3HT and (b) the inverse of the Gaussian line width (σ) from the H-aggregate absorption model. (c) Correlation between the power conversion efficiency and elastic modulus of the P3HT:PCBM films. The number next to each data point refers to the film type in Table 1.

PCBM films. The elastic modulus of the neat P3HT films was determined to be 0.22+/–0.03 GPa and the elastic modulus of the neat PCBM films was determined to be 3.06+/–0.17 GPa. The elastic modulus values compare well to other reports for P3HT of 0.22 GPa[29] and 1.3 GPA,[13] and PCBM of 6.2 GPa.[13] The elastic modulus values of the neat films are found to be independent of annealing at 110 C. On the other hand, the elastic modulus of the P3HT:PCBM blend films are dependent on processing conditions, as shown in **Figure 4** and **Figure 5**.

The elastic modulus of the P3HT:PCBM films was determined to be greater than the classical composite Voigt limit (rule of mixtures), as shown in Figure 4. This synergistic modulus is observed in some polymer-polymer blend films, and is typically seen when there is partial or complete miscibility of the polymers.[41–43] The authors are unaware of any reports of a synergistic modulus composed of a highly loaded small molecule-polymer blend film similar to the P3HT:PCBM films under study. The increased modulus over that predicted by the Voigt model is given by $E = E_1\varphi_1 + E_2\varphi_2 + \beta_{12}\varphi_1\varphi_2$, where E_1 and E_2 are the elastic moduli of components 1 and 2, respectively; and φ_1 and φ_2 are the volume fractions of each component.[42] The interaction term (β_{12}) expresses the magnitude of the deviation from linearity. The modified composite model is fit to the data in Figure 4 for the blend film with the highest elastic modulus using $\beta_{12} = 2.4$ GPa. A synergistic modulus and the level of modulus deviation from the rule of mixtures in polymer blends is typically attributed to an increase in crystallinity of one or both components, modified molecular orientation, the presence of reacted products, and/or a negative volume of mixing.[41,43] In the P3HT:PCBM blend film there are no reaction products between the constituent materials that would contribute to the change in modulus. In addition, the percentage of aggregate P3HT in the neat P3HT films, given in Table S1, is similar to the highly ordered blend films, and thus there is not a dramatic increase in crystallinity that would account for the synergistic modulus. There is however, a possible reduction in volume of the blend film over the pure components. It has recently been noted that annealing a bilayer film of P3HT and PCBM results in mixing of the two materials and a decrease in volume of the stack by approximately 1–2%.[21] While this is a small relative change in thickness, similar changes have been attributed to substantial synergism in the elastic modulus of polymer blends.[43] To determine the extent of a negative volume of mixing, further measurements are required. However it is believed that a negative volume of mixing aided by improved molecular packing is contributing to the synergistic modulus. Note that a large underestimation (overestimation) of the Poisson ratio of P3HT (PCBM) would result in an apparent synergistic modulus. However, given the similar Poisson ratios expected for these materials, this is not believed to contribute to the observed behavior.

The variation in the elastic modulus of the different P3HT:PCBM blend films is attributed to differences in the film order and the magnitude of the negative volume of mixing.

DOI: 10.1002/aenm.201200595

In the blend film, an increase in P3HT crystallinity and local aggregate P3HT order (decrease in σ) is shown to correlate with an increase in elastic modulus in Figure 5. There is also a correlation between the increase in the aggregate P3HT chain length (decrease in *W*) and elastic modulus shown in Figure S2. This suggests that while a change in P3HT crystallinity when going from neat films to blend films is not a dominant feature of the synergistic behavior, the variation in P3HT order in the blend does appear to contribute to the variation in modulus. Processing methods used to increase the percent aggregate P3HT in the blend will result in the mixed amorphous phase becoming increasingly PCBM rich. Increased PCBM in the mixed phase region may result in extending tie-chains between P3HT crystals. This effect combined with improved packing order of the aggregates may reduce the opportunity for polymer movement, contributing to the increase in modulus. This is discussed below in greater detail in the context of film ductility.

The processing methods that allow for an increase in order through molecule reconfiguration during solidification will also provide an opportunity for a negative volume of mixing, and these characteristics are likely coupled. Interestingly, as shown in Figure 4, a fast cast (2,000 rpm) film with a concentration of 38 mg/ml, resulting in a film thickness of 162 nm had the lowest elastic modulus determined in this study and is shown to follow the rule of mixtures closely. This is expected since the film is highly disordered due to the fast spin speed and thinner film resulting in a very fast drying time. This results in poor P3HT local order, which is reflected in the highly disordered absorbance character shown in Figure S5. The fast drying time may also limit efficient molecular packing reducing the chance for a significant negative volume of mixing. Note, it was observed that processing methods used to vary film thickness resulted in systematic variations in the BHJ morphology, as assessed by the absorption spectrum, and correlated variations in the elastic modulus. Additional information on the variation in elastic modulus with thickness is provided in the Supplemental Information.

The elastic modulus is also compared to the power conversion efficiency of OPV devices, shown in Figure 5. The improved film order resulting in the change in absorbance spectra as discussed above also leads to higher device performance. Thus, the elastic modulus and power conversion efficiency follow a similar trend to that of the elastic modulus and P3HT order.

2.3. Crack Onset Strain

In addition to the elastic modulus, the crack onset strain is also critical to the success of flexible organic solar cells. Here, the role of the P3HT:PCBM blend film morphology on the crack onset strain is considered. In this test, the blend film was placed on a PDMS slab and strained in tension under a microscope until the first crack is observed in the film. Images of films showing characteristic fracture behavior are shown in Figure 1. Note, that it has been observed that the crack onset strain in thin films can be dependent on the elastic mismatch between the film and the substrate.[44–46] However, the crack onset strain is insensitive to the substrate material as long as $E_f >> E_S$,[44] which is satisfied for the films under study. The

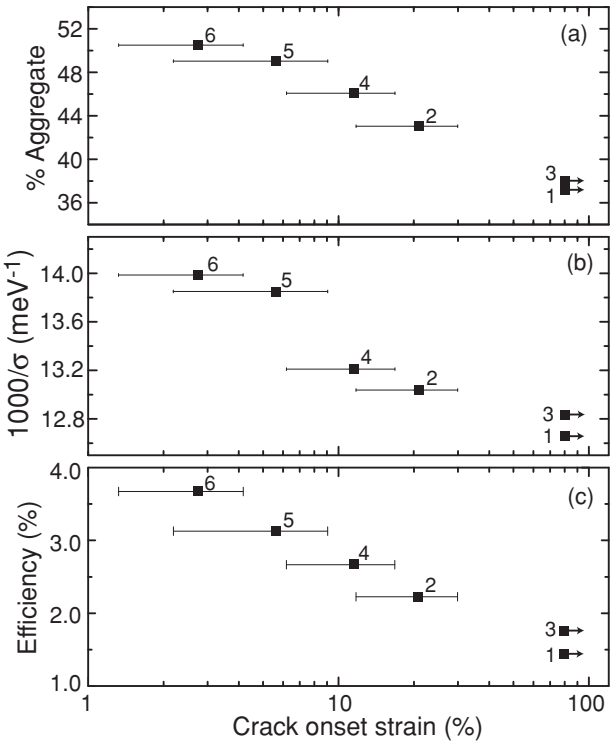

Figure 6. (a-b) Correlations between the crack onset strain and morphology characteristics of P3HT:PCBM blend films including (a) the percent aggregate P3HT and (b) the inverse of the Gaussian line width (σ) from the H-aggregate absorption model. (c) Correlation between the power conversion efficiency and crack onset strain of the blend films. The number next to each data point refers to the film type in Table 1. The arrows next to data points at 80% strain indicate that the PDMS fractured prior to film cracking and the actual crack onset strain is greater than 80%.

measured crack onset strain is compared to the percentage of aggregate P3HT, σ, and OPV power conversion efficiency in **Figure 6**. While cracking is a highly statistical process by nature and analysis through optical microscopy observation is not precise, the change in crack onset strain is clearly apparent, ranging from approximately 2% to over 80%. In the case of the highly ductile films, the PDMS substrate broke before the films cracked.

Straining neat P3HT and PCBM films show the limiting behavior of the P3HT:PCBM blend film. P3HT films are highly ductile and films plastically deform up to the limit of PDMS, similar to previous reports.[47] On the other hand, PCBM films are very brittle and crack under ~2% strain. Both pure films were strained under as-cast, and annealed conditions and no significant difference in crack onset strain was observed. The high ductility of neat P3HT films is expected since its glass transition temperature (T_g) is slightly below room temperature. The T_g of P3HT has been reported from 14 C to 24 C and likely depends on processing methods, molecular weight, and thermal history.[48,49] PCBM has a glass transition temperature much higher than room temperature, reported as 130 C[37] and 148 C,[49] which is consistent with its brittle behavior. The T_g of a P3HT:PCBM blend film with 1:1 ratio by mass is between

these limits with reports of 39 C[48] and 60 C.[49] While these reported glass transition temperatures were determined for very thick drop cast films as opposed to the spun cast films studied here, the glass transition temperatures are expected to be in a similar range.

The blend films in this study are all cast at a 50% relative mass loading; however a large change in ductility is observed. As shown in Figure 6, there is an abrupt change in the crack onset strain from over 80% to approximately 11%, and then a more gradual change from 11% to 2% as film processing increases the percent of aggregate P3HT, and the quality of the aggregates (decrease in σ). There is also a correlation between the conjugation length of the aggregate P3HT (as determined by *W*) and crack onset strain, shown in Figure S4. The ductility of amorphous materials can be highly dependent on temperature, particular near the materials T_g. In the blend films, T_g is a property of the mixed-amorphous regions and thus it should vary with a change in the mixed phase composition. As processing methods are used to improve order within the blend, the aggregated P3HT increases from roughly 35% to 51%. This will result in the mixed amorphous phase becoming increasingly PCBM rich. In addition, the tie chains between P3HT crystals can also limit PCBM miscibility, resulting in the PCBM concentration in regions of the mixed phase even larger than expected from a pure P3HT crystallinity analysis.[21] PCBM swelling the mixed phase region may result in extending the tie-chains between P3HT crystals reducing the opportunity for chain movement. The PCBM rich mixed phase and reduced chain mobility will likely result in an increase in the T_g of the mixed phase. In fact, increasing the loading of PCBM in a P3HT:PCBM blend has been shown to increase the T_g of the film.[48] The increase in T_g will then be reflected in a decrease in ductility at room temperature. In addition, the drop in crack onset strain with decreasing σ suggests that the P3HT aggregate quality also influences the ductility. The smaller Gaussian line width is indicative of a reduction in the stacking faults of the P3HT aggregates, and increase in the planarity of the P3HT chains. This ordering may reduce opportunities for the P3HT to plastically deform by sliding paracrystalline regions and loosely coupled tie-chains, which would be a concurrent effect along with the increase in the percentage of aggregate P3HT. From an alternative perspective, in the highly ordered films, a level of PCBM aggregation may be achieved consistently across the blend film resulting in continuous crack formation with minimal plastic deformation. However, large aggregates of PCBM are not expected to exist in these films.[21]

Differences in the fracture characteristics between films of intermediate and high order are pictured in Figure 1. The highly ordered films show characteristic brittle behavior while films of intermediate order show features of ductile fracture. In the intermediately ordered films, a substantial amount of strain energy is likely dissipated through plastic deformation of the P3HT chains within the mixed phase regions of the film, prior to the chains being fully extended. On the other hand, the P3HT chains in the highly ordered films may already be fully extended removing opportunities for chain movement. This difference in packing character results in the difference in fracture behavior observed.

Note that the variation in strain is quite large, and strains higher than a few percent is due to plastic deformation. While flexible device design should avoid plastic deformation, ductility is important from a durability perspective, where cracking will likely lead to catastrophic OPV device failure.

3. Conclusion

The success of organic solar cells would benefit tremendously from ductile and compliant active layers. In this report, we have shown that in P3HT:PCBM based solar cells, the morphologies that result in high power conversion efficiency have deleterious effect on the mechanical properties: increasing the elastic modulus and lowering the crack onset strain. It was shown that the elastic modulus of the blend film is synergistic, with a value greater than expected using a classical Voigt composite model. The synergistic modulus is attributed to a combination of a negative volume of mixing with contributions from P3HT order in the blend. We also found that disordered P3HT:PCBM films are very ductile similar to neat P3HT films and increasing blend film order results in increasingly brittle behavior. This drastic reduction in ductility is correlated to the increase in both the percent of aggregate P3HT and the local P3HT order. As P3HT order improves, there is a reduction in crystalline stacking faults and loose crystalline tie chains decreasing regions in the film that are likely the origin of plastic deformation. The processing methods that improve P3HT order in the blend film may also raise the glass transition temperature of the film reducing ductility.

While these findings are for P3HT:PCBM films, they are also applicable to other polymer-fullerene systems. For polymer-fullerene BHJs, the morphology must be optimized such that there is intimate mixing of the constituent materials to overcome the limited exciton diffusion length. There also needs to be a level of microstructural order to achieve efficient charge extraction. Other polymer:fullerene systems will likely have a unique relationship between mechanical behavior and device performance; however, optimizing the morphology of other blend films in terms of device performance will likely have a strong influence on their elasticity and ductility. These results compliment previous work that considered the mechanical behavior of P3HT and poly(2,5-bis-(3-dodecylthiophene-2-yl)thieno[3,2-b]thiophenes) (pBTTT), which demonstrated that the interdigitated alkyl side chain packing character of pBTTT that improves long-range order also resulted in an increase in stiffness and decrease in ductility as compared to P3HT.[29] Along with the reported mechanical stability, the variation in morphology may influence other device stability features including chemical[50] and thermal stability.[51,52] For example, previous work has shown that annealing polymer OLEDs can lead to a substantial increase in operational lifetime through improved thermal stability.[52] All factors will be critical for long term operational stability of a flexible organic solar cell. Continued development of conjugated polymers along with the development of device architectures will no doubt continue and detailed analysis of the mechanical behavior will be critical for the ultimate success of flexible organic solar cells.

DOI: 10.1002/aenm.201200595

4. Experimental Section

Certain commercial materials and equipment are identified in the paper to adequately specify the experimental details. In no case does such identification imply recommendation by the National Institute of Standards and Technology, nor does it imply that the material or equipment identified is necessarily the best available for the purpose.

Materials: The P3HT was obtained from Plextronics Inc. with a number-averaged molecular mass Mn = 50 kD, a regioregularity of 99%, and a polydispersity of 2.1. The PCBM was obtained from Nano-C with a purity of 99%. The PEDOT:PSS solution was type PVP AI4083, obtained from Heraeus Materials Technology.

Film preparation: The P3HT:PCBM bulk heterojunction films are spin cast on silicon, and ITO coated glass substrates pre-coated with a PEDOT:PSS film. The P3HT:PCBM with a 1:1 mass ratio is dissolved in 1,2-dichlorobenzene (DCB) at different loadings including 26, 30, 34, 38, 45 and 50 mg ml^{-1}. The solutions are prepared in a nitrogen filled glovebox and are placed on a hotplate at 75 C for a minimum of 12 hours and then allowed to cool down to room temperature before casting. All substrates are cleaned by sonication for 10 minutes in deionized (DI) water, acetone and isopropynol, followed by UV-ozone treatment for 10 minutes, and rinse with DI water. Prior to casting the BHJ film, PEDOT:PSS films are spun cast onto the substrates. The PEDOT:PSS films are cast at 5,000 rpm for 60 s and then annealed inside a glovebox at 120 C for 20 minutes. The P3HT:PCBM is then cast on the PEDOT:PSS at varying spin speeds ranging from 600 rpm to 2,000 rpm for 60 s to achieve the desired thickness. After casting the P3HT:PCBM films, they are either left "as-cast" or "annealed". The as-cast films are removed from the spin coater and left in the glove box uncovered for a minimum of 30 minutes. After casting the films, the annealed films are immediately covered under a Petri dish for 20-minutes. The films cast at lower spin speeds (600 and 1,000 rpm) remained partially wet at the edges when placed under the Petri dish resulting in a solvent anneal effect. All annealed films were then thermally annealed on a hot plate at 110 C for 20 minutes. The neat P3HT and PCBM films were spun coat at 1,000 rpm from 20 mg ml^{-1} and 30 mg ml^{-1} DCB solutions respectively. For solar cells, the blend films are cast on PEDOT:PSS coated ITO-glass substrates with a sheet resistance of 8–12 Ohms sq^{-1}. The cathode is deposited by vacuum thermal evaporation at a pressure of 1×10^{-6} torr. The cathode consists of ~1 nm lithium fluoride and ~100 nm aluminum film.

Characterization: The thickness of the films is determined using a Woollam variable-angle spectroscopic ellipsometer (VASE). A 5 phase (ambient, BHJ, pedot, oxide, silicon) model is used. To allow for variations in the optical properties due to processing, the BHJ was modeled using an isotropic Cauchy fit over the optical range of 750–1100 nm with both thickness and Cauchy parameters fit. This fit was compared to a uniaxial EMA model for the BHJ based on reference P3HT and PCBM functions using the spectrum between 400–1100 nm resulting in thickness estimates within 3 nm of each other.[23] Absorbance measurements are made using an Ocean Optics Jazz spectrometer. Absorbance was measured on P3HT:PCBM films cast on PEDOT:PSS, ITO-glass substrates. The organic photovoltaic devices are tested using a Newport 150 W solar simulator with an AM1.5G filter under 100 mW cm^{-2} as determined by an NREL traceable un-filtered Si-diode. The OPV device area is 3.14 mm^2, and the device performance is not corrected for spectral mismatch. The reported device performance is for the best performing cell for each casting condition.

Buckling and crack onset strain measurements: All films are cast on PEDOT:PSS coated silicon substrates. The films are then laminated onto a pre-strained (~10%) PDMS slab and submerged into DI water. The PEDOT:PSS dissolves in the water bath after several hours detaching the silicon substrate and leaving the thin film alone on the PDMS substrate. The thin film-PDMS stack is then thoroughly dried with nitrogen gas. The tensile strain is slightly removed from the PDMS placing the thin film in compression resulting in a linear buckling pattern. The elastic modulus is determined by taking the average buckling wavelength of the film in approximately six locations. The average wavelength is then used along with the film thickness as measured using spectroscopic ellipsometry to determine the elastic modulus for each film. The reported elastic modulus for similarly processed films is an average of at least three films, and the reported uncertainty is the standard deviation of the mean. The PDMS was approximately 2 mm thick, cast with a base to crosslinker ratio of 15:1, and cured at a temperature of 60 C for over 12 h. The elastic modulus of the PDMS substrate is determined using an Instron 5943 tensile tester. The PDMS modulus was determined for each PDMS slab used in the buckling measurements and varied between 0.66 MPa and 0.73 MPa. For the brittle films, the compressive strain used for buckling is held below levels that result in film cracking. The crack onset strain is determined by applying a tensile strain to the thin film-PDMS composite and observing crack initiation using an optical microscope. The reported crack onset strain is an average measured value from a minimum of 4 films for each blend film processing condition, and 2 films for the neat P3HT and PCBM films. The error bars in the crack onset strain represent one standard deviation of the data, which is taken as the experimental uncertainty of the measurement.

Supporting Information

Supporting Information is available from the Wiley Online Library or from the author.

Acknowledgements

The authors would like to thank Dr. Jan Genzer for assistance with ellipsometry measurements, and Dr. Michael Dickey for assistance with tensile testing the PDMS substrates. This material is based upon work supported by the National Science Foundation under Grant No. CMMI-1200340. B.I.L. acknowledges support from NIST/NSF Summer Undergraduate Research Fellowship.

Received: August 3, 2012
Published online:

[1] C. J. Brabec, S. Gowrisanker, J. J. M. Halls, D. Laird, S. Jia, S. P. Williams, *Adv. Mater.* **2010**, *22*, 3839.
[2] C. Deibel, V. Dyakonov, *Rep. Prog. Phys.* **2010**, *73*, 096401.
[3] J. Hou, H. Y. Chen, S. Zhang, R. I. Chen, Y. Yang, Y. Wu, G. Li, *J. Am. Chem. Soc.* **2009**, *131*, 15586–15587.
[4] A. A Bakulin, A. Rao, V. G. Pavelyev, P. H. M. van Loosdrecht, M. S. Pshenichnikov, D. Niedzialek, J. Cornil, D. Beljonne, R. H. Friend, *Science* **2012**, *1340*.
[5] B. A. Collins, J. R. Tumbleston, H. Ade, *J. Phys. Chem. Lett.* **2011**, *2*, 3135.
[6] M. R. Hammond, R. J. Kline, A. A. Herzing, L. J. Richter, D. S. Germack, H. Ro, C. L. Soles, D. A. Fischer, T. Xu, L. Yu, M. F. Toney, D. M. Delongchamp, *ACS Nano* **2011**, *5*, 8248.
[7] T. Han, Y. Lee, M. Choi, S. Woo, S. Bae, B. H. Hong, J. Ahn, T. Lee, *Nat. Photon.* **2012**, *6*, 105.
[8] G. H. Gelinck, H. E. Huitema, E. van Veenendaal, E. Cantatore, L. Schrijnemakers, J. B. P. H. van der Putten, T. C. T. Geuns, M. Beenhakkers, J. B. Giesbers, B. H. Huisman, E. J. Meijer, E. M. Benito, F. J. Touwslager, A. W. Marsman, B. J. E. van Rens, D. M. de Leeuw, *Nat. Mater.* **2004**, *3*, 106.
[9] G. Dennler, C. Lungenschmied, H. Neugebauer, N. S. Sariciftci, M. Latrèche, G. Czeremuszkin, M. R. Wertheimer, *Thin Solid Films* **2006**, *511*, 349.
[10] J. Lewis, *Mater. Today* **2006**, *9*, 38.

[11] D. R. Cairns, R. P. Witte, D. K. Sparacin, S. M. Sachsman, D. C. Paine, G. P. Crawford, R. R. Newton, *App. Phys. Lett.* **2000**, *76*, 1425.
[12] S. R. Dupont, M. Oliver, F. C. Krebs, R. H. Dauskardt, *Sol. Energy. Mater. Sol. Cells* **2012**, *97*, 171.
[13] D. Khang, J. A. Rogers, H. H. Lee, *Adv. Funct. Mater.* **2009**, *19*, 1526.
[14] P. G. Karagiannidis, S. Kassavetis, C. Pitsalidis, S. Logothetidis, *Thin Solid Films* **2011**, *519*, 4105.
[15] Y. Kim, S. A. Choulis, J. Nelson, D. D. C. Bradley, S. Cook, J. R. Durrant, *App. Phys. Lett.* **2005**, *86*, 063502.
[16] G. Li, V. Shrotriya, J. Huang, Y. Yao, T. Moriarty, K. Emery, Y. Yang, *Nat. Mater.* **2005**, *4*, 864.
[17] J. Y. Chung, J. H. Lee, K. L. Beers, C. M. Stafford, *Nano letters* **2011**, *11*, 3361.
[18] D. Tahk, H. H. Lee, D. Y. Khang, *Macromolecules*. **2009**, *42*, 7079.
[19] D. Chen, A. Nakahara, D. Wei, D. Nordlund, T. P. Russell, *Nano letters* **2011**, *11*, 561.
[20] S. T. Turner, P. Pingel, R. Steyrleuthner, E. J. W. Crossland, S. Ludwigs, D. Neher, *Adv. Funct. Mater.* **2011**, *21*, 4640.
[21] H. Ro, B. Akgun, B. T. O'Connor, M. Hammond, R. J. Kline, C. R. Snyder, S. K. Satija, A. L. Ayzner, M. F. Toney, C. L. Soles, D. M. DeLongchamp, *Macromolecules* **2012**, *45*, 6587.
[22] S. van Bavel, E. Sourty, G. de With, K. Frolic, J. Loos, *Macromolecules* **2009**, *42*, 7396.
[23] D. S. Germack, C. K. Chan, R. J. Kline, D. A. Fischer, D. J. Gundlach, M. F. Toney, L. J. Richter, D. M. DeLongchamp, *Macromolecules* **2010**, *43*, 3828.
[24] M. Campoy-Quiles, T. Ferenczi, T. Agostinelli, P. G. Etchegoin, Y. Kim, t. D. Anthopoulos, P. N. Stavrinou, D. D. C. Bradley, J. Nelson, *Nat. Mater.* **2008**, *7*, 158.
[25] J. K. Lee, W. L. Ma, C. J. Brabec, J. Yuen, J. S. Moon, J. Y. Kim, K. Lee, G. C. Bazan, A. J. Heeger, *J. Am. Chem. Soc.* **2008**, *130*, 3619.
[26] J. Peet, J. Y. Kim, N. E. Coates, W. L. Ma, D. Moses, A. J. Heeger, G. C. Bazan, *Nat. Mater.* **2007**, *6*, 497–500.
[27] C. M. Stafford, C. Harrison, K. L. Beers, A. Karim, E. J. Amis, M. R. Vanlandingham, H. C. Kim, W. Volksen, R. D. Miller, E. W. Simonyi, *Nat. Mater.* **2004**, *3*, 545.
[28] P. Murugavel, C. Narayana, A. Govindaraj, A. K. Sood, *Chem. Phys. Lett.* **2000**, *331*, 149.
[29] B. O'Connor, E. P. Chan, C. Chan, B. R. Conrad, L. J. Richter, R. J. Kline, M. Heeney, I. McCulloch, C. L. Soles, D. M. DeLongchamp, *ACS Nano* **2010**, *4*, 7538.
[30] Y. Leterrier, L. Medico, F. Demarco, J. A. E. Manson, U. Betz, M. F. Escola, M. K. Olsson, F. Atamny, *Thin Solid Films* **2004**, *460*, 156.
[31] L. F. Drummy, R. J. Davis, D. L. Moore, M. Durstock, R. A. Vaia, J. W. P. Hsu, *Chem. Mater.* **2011**, *23*, 907.
[32] A. J. Parnell, A. J. Cadby, O. O. Mykhaylyk, A. D. F. Dunbar, P. E. Hopkinson, A. M. Donald, R. A. L. Jones, *Macromolecules* **2011**, *44*, 6503.
[33] F. C. Spano, *J. Chem. Phys.* **2005**, *122*, 234701.
[34] U. Zhokhavets, T. Erb, G. Gobsch, M. Al-Ibrahim, O. Ambacher, *Chem. Phys. Lett.* **2006**, *418*, 347.
[35] J. Clark, J. F. Chang, F. Spano, R. H. Friend, C. Silva, *Appl. Phys. Lett.* **2009**, *94*, 163306.
[36] B. A. Collins, E. Gann, L. Guignard, X. He, C. R. McNeill, H. Ade, *J. Phys. Chem. Lett.* **2010**, *1*, 3160.
[37] E. Verploegen, R. Mondal, C. J. Bettinger, S. Sok, M. F. Toney, Z. A. Bao, *Adv. Funct. Mater.* **2010**, *20*, 3519.
[38] G. Dennler, K. Forberich, M. C. Scharber, C. J. Brabec, I. Tomis, K. Hingerl, T. Fromherz, *J. Appl. Phys.* **2007**, *102*, 054516.
[39] B. O'Connor, C. Haughn, K. H. An, K. P. Pipe, M. Shtein, *Appl. Phys. Lett.* **2008**, *93*, 223304.
[40] D. Chirvase, J. Parisi, J. C. Hummelen, V. Dyakonov, *Nanotechnology* **2004**, *15*, 1317.
[41] A. Granado, J. I. Equizabal, J. Nazabal, *Macromol. Mater. Eng.* **2004**, *289*, 281.
[42] B. Nandan, L. D. Kandpal, G. N. Mathur, *J. Appl. Polym. Sci.* **2003**, *90*, 2887.
[43] J. Ramiro, J. I. Eguiazabal, J. Nazabal, *Polym. Advan. Technol.* **2003**, *14*, 129.
[44] J. H. Lee, J. Y. Chung, C. M. Stafford, *ACS Macro Lett.* **2012**, *1*, 122.
[45] J. H. Waller, L. Lalande, Y. Leterrier, J. A. E. Manson, *Thin Solid Films* **2011**, *519*, 4249.
[46] N. J. Douville, Z. Y. Li, S. Takayama, M. D. Thouless, *Soft. Matter.* **2011**, *7*, 6493.
[47] B. O'Connor, R. J. Kline, B. R. Conrad, L. J. Richter, D. Gundlach, M. F. Toney, D. M. DeLongchamp, *Adv. Funct. Mater.* **2011**, *21*, 3697.
[48] J. Y. Kim, D. Frisbie, *J. Phys. Chem. C.* **2008**, *112*, 17726.
[49] J. Zhao, A. Swinnen, G. van Assche, J. Manca, D. Vanderzande, B. van Mele, *J. Phys. Chem. B.* **2009**, *113*, 1587.
[50] K. Lee, J. Y. Kim, S. H. Park, S. H. Kim, S. Cho, A. J. Heeger, *Adv. Mater.* **2007**, *19*, 2445.
[51] T. W. Lee, O. O. Park, *Adv. Mater.* **2000**, *12*, 801.
[52] J. Kim, J. Lee, C. W. Han, N. Y. Lee, I. J. Chung, *App. Phys. Lett.* **2003**, *82*, 4238.

Adv. Energy Mater. **2012**,
DOI: 10.1002/aenm.201200595